Journal of Power Sources 200 (2012) 34–44

Contents lists available at SciVerse ScienceDirect

Journal of Power Sources

journal homepage: www.elsevier.com/locate/jpowsour

Design and technoeconomic performance analysis of a 1 MW solid oxide fuel cell polygeneration system for combined production of heat, hydrogen, and power

W.L. Becker[a], R.J. Braun[a,*], M. Penev[b], M. Melaina[b]

[a] Mechanical Engineering Department, Colorado School of Mines, Golden, CO, USA
[b] Hydrogen Technologies & Systems Center, National Renewable Energy Laboratory, Golden, CO, USA

ARTICLE INFO

Article history:
Received 23 August 2011
Received in revised form 11 October 2011
Accepted 11 October 2011
Available online 18 October 2011

Keywords:
Solid oxide fuel cells
Combined heat and power
Polygeneration
Hydrogen production
System analysis
Distributed generation

ABSTRACT

This work focuses on the design and performance estimation of a methane-fueled, 1 MW SOFC combined heat, hydrogen, and power (CHHP) system operating at steady-state. Two methods of hydrogen purification and recovery from the SOFC tail-gas are analyzed: pressure swing adsorption (PSA) and electrochemical hydrogen separation (EHS). The SOFC electrical efficiency at rated power is estimated at 48.8% (LHV) and the overall CHHP efficiency is 85.2% (LHV) for the EHS design concept. The EHS energy requirement of 2.7 kWh kg^{-1} H_2 is found to be about three times lower than PSA in this system. Operating the system to produce additional hydrogen by flowing excess methane into the SOFC subsystem results in increased efficiency for both of the hydrogen separation design concepts. An economic analysis indicates that the expected cost of SOFC-based distributed hydrogen production (4.4 $ kg^{-1}) is on par with other distributed hydrogen production technologies, such as natural gas reforming, electrolysis, and molten carbonate fuel cell CHHP systems. The study illustrates that 'spark spreads' (cost of electricity in ¢ kWh^{-1} minus cost of natural gas in $ $MMBtu^{-1}$) of five or more offer near-zero or negative hydrogen production costs for distributed SOFC CHHP plants with total installed capital costs near 3950 $ kW.

1. Introduction

Distributed energy generation is necessary to integrate both renewable and higher efficiency generators into the energy infrastructure. Solid oxide fuel cell (SOFC) systems can be fueled by natural gas or hydrogen to produce electric power, and they exhibit high overall efficiency when co-generation is used. Co-generation studies have typically focused on electricity and heat; pure hydrogen gas can also be generated in these systems as an energy co-product resulting in the combined production of heat, hydrogen, and power (CHHP). Co-locating a distributed generation SOFC CHHP plant with fueling stations for fuel cell vehicles enables use of lower-scale (250–350 kg day^{-1}) hydrogen production and leverages the capital investment among all co-products, thereby lowering the unit cost of hydrogen and offering a potentially promising transition pathway to a hydrogen economy. With respect to carbon dioxide emissions from fossil fuels, natural gas is one of the cleanest to combust. Hydrogen fuel produced from wind or photovoltaic-powered electrolysis would make the SOFC system renewable and carbon free. At present, the resource most readily available for fueling an SOFC system is natural gas; this fuel, modeled as pure methane, is chosen in the present study.

Electrochemical hydrogen separation (EHS) employs proton conducting electrolytic cells in which an applied potential drives hydrogen to oxidize to H^+ at the anode, diffuse through the electrolyte membrane, and reduce back to H_2 at the cathode. Fig. 1 illustrates the separation mechanism. The result is a pure hydrogen gas stream exiting the cathode. This process has been shown to be suitable for methane reformate gas streams with a high degree of separation, high purity hydrogen, and relatively small power requirements [1,2]. PEM electrolytic cells using polybenzimidazole (PBI) membranes operate at temperatures of 160–200 °C and are able to tolerate levels of CO up to around 1.5%, which is above the CO content in typical water-gas shifted anode effluent gas streams. Although the presence of CO hinders the performance of the cell due to poisoning, operating at higher temperatures (up to 200 °C) reduces the poisoning effect, and sustained (4000 h) performance has been demonstrated [2].

One issue associated with EHS technology is membrane crossover of CO and CO_2 which reduces the hydrogen purity at the cathode. Recent advancements in EHS technology have achieved a 150 and 62 fold reduction (factor of gas species found in the cathode stream compared to the anode) in crossover CO and CO_2, respectively [2]. However, this reduction does not result in sufficient hydrogen purity for PEM fuel cells. Depending on the catalyst

* Corresponding author. Tel.: +1 303 273 3055; fax: +1 303 273 3055.
E-mail address: rbraun@mines.edu (R.J. Braun).

0378-7753/$ – see front matter © 2011 Elsevier B.V. All rights reserved.
doi:10.1016/j.jpowsour.2011.10.040

Nomenclature

V	cell voltage (V)
OCV	open circuit voltage
η_{act}	activation polarization loss (V)
η_{ohm}	ohmic polarization loss (V)
η_{conc}	concentration polarization loss (V)
E	Nernst voltage (V)
E_o	reference voltage (V)
R	universal gas constant (J (mol K)$^{-1}$)
T	cell temperature (°C)
F	Faraday's constant (J mol^{-1})
N	number of electrons per mol
P_i	partial pressure of component i (atm)
P	pressure (psi)
θ	experimental to Nernst OCV fraction
OCV_{exp}	experimental open circuit voltage (V)
OCV_{Nernst}	theoretical open circuit voltage (V)
J	current density (A cm^{-2})
J_o	exchange current density (A cm^{-2})
A	apparent charge transfer coefficient
Γ	activation overpotential factor(A cm^{-2})
E_{act}	activation energy (J mol^{-1})
ASR_{ohm}	area specific resistance (Ω cm^2)
j_L	limiting current density (A cm^{-2})
P_{DC}	gross DC power from SOFC (kW)
A_{tot}	total SOFC active area required (cm^2)
N_{cells}	number of cells
A_{cell}	area of a cell (cm^2)
N_{stacks}	number of stacks
U_f	fuel utilization
LHV	lower heating value (kW)
HHV	higher heating value (kW)

used in the PBI separation unit, the water gas shift reaction could occur at these low temperatures which could further reduce the CO content in the anode. According to one manufacturer [3], a CO reduction of 10,000:1 can be realized which would purify the hydrogen gas to the necessary limit of 1–2 ppmv.

Pressure swing adsorption (PSA) is used in industry, especially in oil refineries, to separate hydrogen from steam methane reforming (SMR) gas streams. Product hydrogen purities greater than 99.99% can be achieved through this process, but the amount of hydrogen recovered decreases substantially with lower hydrogen content in the inlet gas (<70%, molar basis) [4]. The effluent of SOFC generators with fuel utilizations of about 80% will have lower hydrogen content than SMR effluent (e.g., ~20% versus ~70%, molar basis). For an SOFC system operating at atmospheric pressure, there is no reduction in compression energy by using PSA for hydrogen separation. The composition of hydrogen at the inlet of the PSA unit must be 70% or higher for the process to be economical and achieve 85% separation [5,6].

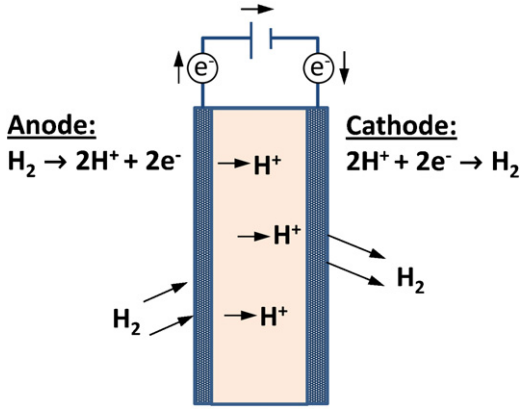

Fig. 1. Electrochemical hydrogen separation membrane showing electrode half reactions, electron conduction, and proton diffusion through the electrolyte [2].

There are several studies [7,8] that have examined the co-production of hydrogen in addition to power and heat from SOFC systems. Mitlitsky [7] performed a study integrating an SOFC module with an EHS unit. Although this study employed a smaller-scale fuel cell (25 kWe AC with a maximum hydrogen production of 19 kg day^{-1}) than the system in the present study, the EHS units are scalable in the same manner as fuel cells. In fact, the EHS performance is predicted to improve with increased size [7]. The product hydrogen gas is intended for use in low-temperature PEM fuel cells, so the limit of CO in the hydrogen stream is in the range of 1–2 ppmv. The EHS unit in Ref. [7] demonstrated a 2600:1 reduction of CO in the product stream, which would purify the hydrogen from a feed CO content of 0.5% down to 1–2 ppmv.

Another study [8] examined the tri-generation of heat, hydrogen and power by using a combination of an SOFC and a solid oxide electrolyzer cell (SOEC). The methane-fueled SOFC provided electricity and heat to the SOEC for hydrogen production, and the SOFC tail-gas was combusted with the oxygen-enriched sweep gas of the SOEC for heat recovery. The operation and control of such a system would be difficult due to the inherent feedback and dependence between the two subsystems.

The goal of this study is to estimate the steady-state performance and costs of a 1 MW SOFC CHHP system using two different methods for hydrogen separation: electrochemical hydrogen pumping and pressure swing adsorption. The results give insight into the potential scenarios for operation of such systems and the associated economic implications in terms of cost of hydrogen.

In this paper, the modeling methodology employed is first discussed, which is inclusive of an overview of the plant process diagram. Next, model results and discussion are given for two design concepts which are differentiated by the method in which they purify the SOFC tail-gas: (1) SOFC integrated with EHS and (2) SOFC integrated with PSA. An operational variation of producing excess hydrogen for both concepts is then presented. A technoeconomic analysis of the CHHP system is also presented in which a bottom-up plant cost estimate is presented and the sensitivity of the cost of hydrogen to variations in the value of the co-products is explored. Finally, conclusions are given with the preferred design concept and future analyses for this system are suggested.

2. Modeling methodology

Fig. 2 illustrates the first design concept (Concept 1) of the CHHP system. Methane enters at state-point (1) and is compressed before mixing with the anode recycle gases. The fuel mixture is then heated in HX-01 before pre-reforming. The gas is heated a second time and enters the anode of the SOFC at state-point (6). The heat from the anode effluent is exchanged with both the anode and pre-reformer inlet gas streams. Part of the gas stream is then recycled, and the rest (10) gets cooled to a temperature (300 °C) suitable for the water gas shift (WGS) reactor. The heat from the WGS reactor effluent is partially recovered in the hot water loop (32–33–34–35) before entering the EHS unit. The recovered hydrogen (30) is compressed to 30 bar for transport to a storage and dispensing facility. The EHS tail gas (16) is combusted with part of the cathode effluent (air). The combustor effluent exchanges heat with the water loop in HX-06 before being exhausted (29) at 92 °C. The air for the

cathode enters at (19) and undergoes the bulk of its preheating in HX-04 before entering the cathode (22) at about 650 °C. The cathode effluent heat is recuperated in HX-04 and is then sent to the combustor. Part of the cathode effluent (25) is used for combustion, and the rest is bypassed before exchanging heat with the water loop in HX-06.

Fig. 3 illustrates the second design concept (Concept 2). The differences between these concepts are evident in the hardware downstream of the water gas shift reactor (14). The shifted anode effluent heat is partially recovered to the water loop in HX-05, and a fraction of the water is condensed out. Most of the remaining water is then drained in the condenser so that the PSA compressor inlet gas mixture contains less than 0.3% water vapor (by volume). The gas is compressed and sent to the inlet (20) of the PSA unit. Part of the hydrogen which is separated by the PSA unit is recycled back to the inlet to achieve the designated inlet composition (as described later), and the remaining hydrogen stream (26) is compressed to 30 bar. The PSA tail-gas is sent to the combustor, by which heat is recovered in HX-06 as described in Concept 1.

Models of each of the two system concepts were developed in Aspen Plus™ required to carryout the thermo-chemical analysis at the desired fidelity. The following sections describe the processes of the plant in more detail.

2.1. Fuel and air inlet

Methane and air are fed into the system and compressed to 20 kPa above atmospheric pressure to account for pressure loss of the system. The fresh methane feed is mixed with recycled anode exhaust gas, which is used to ensure a steam-to-methane ratio of about 2.9 at the pre-reformer inlet. Water production at the anode along with 65% anode recycle is sufficient to meet the steam-to-carbon ratio requirement; a ternary diagram analysis for hydrogen, carbon and oxygen atoms indicates that carbon deposition is not thermodynamically favorable for the pre-reformer and anode operating conditions. Air supply is determined by the amount of cooling needed in the stack. An air stoichiometric factor for the system, defined as the ratio of oxygen fed into the cathode to the oxygen that is electrochemically reduced, is about 3.3 to limit the temperature rise of the stack to 150 °C.

2.2. Fuel processing and preheat

The fuel mixture is preheated to 700 °C for partial catalytic steam methane reforming (SMR). Pre-reforming of the methane is beneficial to both limit the solid temperature gradient in the stack and to reduce the tendency for carbon formation due to the presence of higher hydrocarbons in natural gas and the lack of hydrogen at the cell inlet. The endothermic SMR reaction typically occurs near the inlet of the cell, and the coinciding exothermic electrochemical oxidation of hydrogen causes a steep temperature gradient down the length of the cell. By limiting the amount of direct internal reforming, the temperature gradient will be reduced. Pre-reforming 20% of the CH_4 in the fuel mixture is specified for the present model. Most of the fuel preheating is accomplished by recuperation of the anode effluent, but excess methane (stream 17 in Fig. 2) is fed into the burner if this heat is not sufficient (for example, in Concept 1). The endothermic reforming lowers the temperature of the fuel stream, so another heat exchanger is used to bring the anode inlet stream up to 650 °C. All of the heat exchangers in the model are designed to have a 10 °C minimum temperature approach; the additional fuel fed into the combustor for SMR preheating (HX-01) was controlled by this criterion. The total heat loss for the plant is modeled to be 2.5% of the LHV of the methane feed. Table 1 summarizes the distribution of heat loss throughout the plant.

Table 1
Heat loss in %LHV of methane feed.

Pre-reformer	0.25%
SOFC	1.0%
WGS reactor	0.25%
Combustor	0.5%
System piping	0.5%

This results in about 5 kW of heat loss for the pre-reformer and WGS reactor, 10 kW for the combustor and system piping, and 20 kW for the SOFC.

2.3. Air preheat

The air must also be preheated to 650 °C to avoid mechanical failure of the stack arising from excessive solid temperature gradients. Air preheating also improves the kinetics of the oxygen reduction reaction. The air is partially heated (from 20 °C to about 80 °C) in HX-03 which is used to cool the non-recycled anode exhaust to a temperature favorable for the water gas shift reaction (300 °C). The bulk of the air heating occurs in a cathode feed-exhaust recuperation heat exchanger (HX-04).

2.4. Solid oxide fuel cell

The SOFC was modeled as a black box component designed to operate at a chosen voltage and fuel utilization. Modeling parameters for the SOFC performance were chosen from the literature [9]. The fuel cell operating conditions were modeled based on the average temperature and fuel composition of the inlet and outlet. The nominal operating temperature of the stack is estimated to be 725 °C with a per-pass fuel utilization of 62.5%. The polarization curve was calculated from

$$V = \mathrm{OCV} - \eta_{act} - \eta_{ohm} - \eta_{conc} \tag{1}$$

where OCV is the open circuit voltage, and the η terms are the activation, ohmic and concentration losses described below. The OCV takes into account the temperature and composition dependence of the Nernst voltage, as well as the deviation of the experimental OCV voltage from theory according to

$$E = E_o + \frac{RT}{nF}\, ln\left[\frac{P_{H_2} P_{O_2}^{0.5}}{P_{H_2O} P_{atm}^{0.5}}\right] \tag{2}$$

where from [10]

$$E_o = 1.2723 - 2.7645 \times 10^{-4} \times T \tag{3}$$

and $n = 2$ and $F = 96485\ \mathrm{J\,mol^{-1}}$. Deviation of the experimental OCV from the Nernst voltage is accounted for by

$$\theta = \frac{\mathrm{OCV}_{exp}}{\mathrm{OCV}_{Nernst}} \tag{4}$$

where θ accounts for electronic and ionic conductivity of the electrolyte at open circuit conditions [11]. This factor is approximated to be 0.94 [11]. The activation polarization, η_{act}, is implicitly determined from the Butler–Volmer equation:

$$j = j_o\left[exp\left(\alpha\frac{nF}{RT}\eta_{act}\right) - exp\left(-(1-\alpha)\frac{nF}{RT}\eta_{act}\right)\right] \tag{5}$$

where α is the charge transfer coefficient, and j_o is a pre-exponential factor that is specific to each electrode as given by

$$j_{o,c} = \gamma_c\left(\frac{P_{O_2}}{P_{atm}}\right)^{0.25} exp\left(-\frac{E_{act,c}}{RT}\right) \tag{6}$$

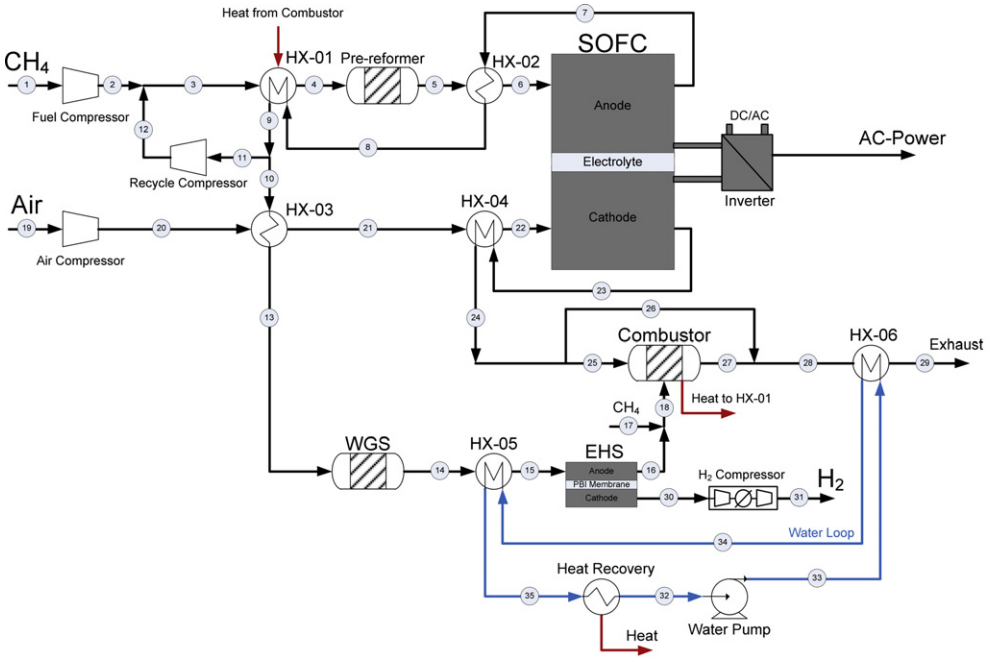

	T (°C)	P (kPa)	ṁ (kg/s)
1	20	101	0.039
2	37	122	0.039
3	484	115	0.349
4	700	112	0.349
5	568	109	0.349
6	658	108	0.349
7	750	103	0.477
8	676	101	0.477
9	533	100	0.477
10	533	100	0.167
11	533	100	0.310
12	581	115	0.310
13	300	98	0.167
14	343	95	0.167
15	190	94	0.167
16	190	94	0.164
17	30	101	0.003
18	184	94	0.167
19	20	101	1.849
20	45	122	1.849
21	80	121	1.849
22	654	119	1.849
23	800	114	1.721
24	201	113	1.721
25	201	113	1.592
26	201	113	0.129
27	676	90	0.296
28	294	90	1.888
29	92	89	1.888
30	70	136	0.003
31	70	3039	0.003
32	60	207	5.372
33	60	276	5.372
34	78	241	5.372
35	80	207	5.372

Fig. 2. Concept 1: SOFC CHHP with EHS and table of state points.

$$j_{o,a} = \gamma_a \left(\frac{P_{H_2}}{P_{atm}}\right)\left(\frac{P_{H_2O}}{P_{atm}}\right) exp\left(-\frac{E_{act,a}}{RT}\right) \quad (7)$$

where γ is an activation overpotential factor and E_{act} is the activation energy; these values are obtained from [13]. The charge transfer coefficient, α, typically ranges from 0.2 to 0.5 [14]. For reversible reactions (a typical assumption made for SOFC kinetic behavior), the chemical and electrical energy form equal activation barriers for the forward and reverse reactions, so $\alpha = 0.5$ [14]; this simplification is used to reduce the B–V equation (5) to

$$j = 2j_o \ sinh\left(\frac{nF}{2RT}\eta_{act}\right) \quad (8)$$

The ohmic loss term, η_{ohm}, is dependent on both the resistivity of the stack components, and their thicknesses. An area specific resistance can be used as an approximation for this dependence

$$\eta_{ohm} = j \times ASR_{ohm} \quad (9)$$

where ASR_{ohm} is the ohmic area specific resistance estimated from Ref. [14] to be $0.04\,\Omega\,cm^2$. The concentration losses, η_{conc}, is determined by the limiting current density in the following relationship:

$$\eta_{conc} = \frac{RT}{nF} ln\left(1 - \frac{j}{j_L}\right) \quad (10)$$

where j_L is the limiting current density and is estimated to be $1.6\,A\,cm^{-2}$ at 800 °C from [9].

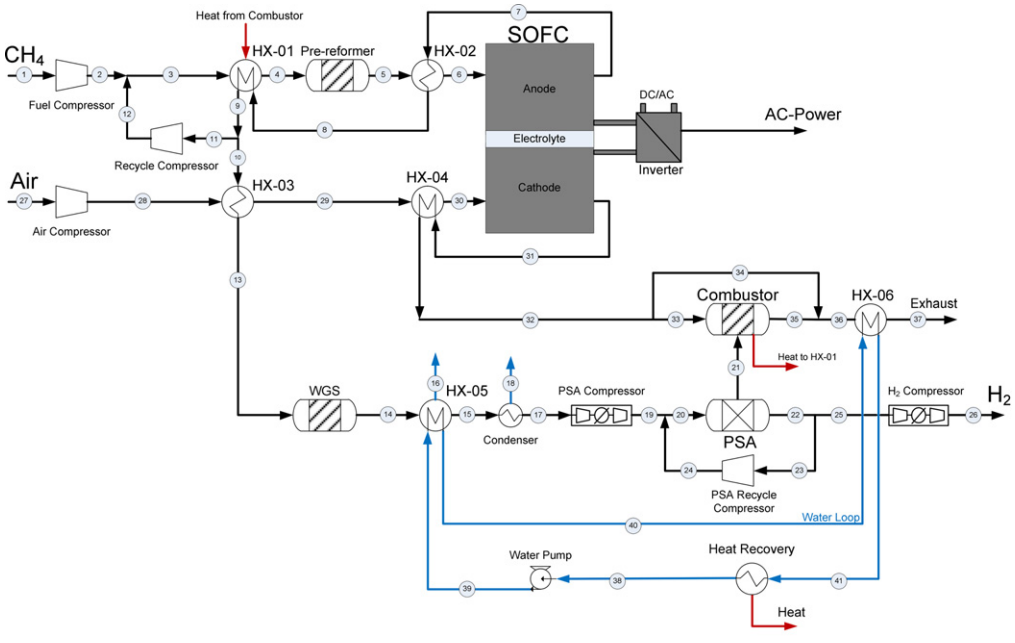

	T (°C)	P (kPa)	ṁ (kg/s)
1	20	101	0.039
2	37	122	0.039
3	478	122	0.349
4	700	119	0.349
5	568	116	0.349
6	658	114	0.349
7	750	109	0.477
8	676	108	0.477
9	529	107	0.477
10	529	107	0.167
11	529	107	0.310
12	574	122	0.310
13	301	105	0.167
14	344	102	0.167
15	104	100	0.147
16	104	100	0.020
17	40	100	0.109
18	40	100	0.038
19	50	1772	0.109
20	53	1772	0.118
21	53	1772	0.108
22	53	1720	0.010
23	53	1720	0.008
24	56	1772	0.008
25	53	1720	0.002
26	70	3039	0.002
27	20	101	1.849
28	45	122	1.849
29	79	121	1.849
30	655	119	1.849
31	801	114	1.721
32	201	113	1.721
33	201	113	0.103
34	201	113	1.618
35	845	98	0.211
36	286	98	1.828
37	115	97	1.828
38	60	207	5.215
39	60	276	5.215
40	65	241	5.215
41	80	207	5.215

Fig. 3. Concept 2: SOFC CHHP with PSA and table of state points.

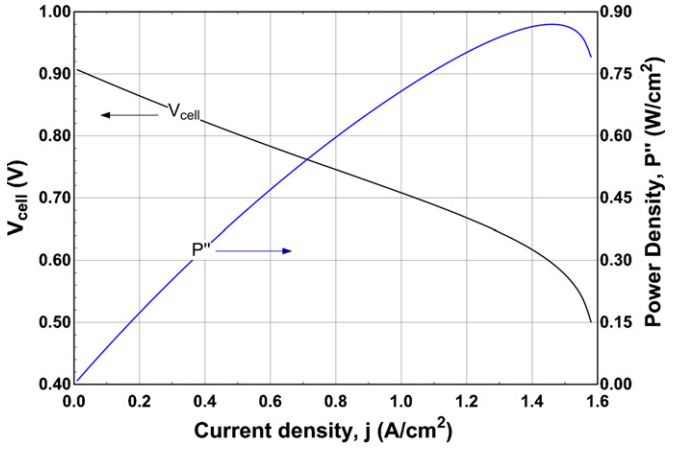

Fig. 4. SOFC polarization curve and power density for average temperature of 725 °C, atmospheric pressure, and average composition of 50% H_2, 42% H_2O at the anode and 18.4% O_2 at the cathode.

Fig. 4 illustrates the polarization curve for the modeled fuel cell operating at an average temperature of 725 °C, atmospheric pressure, fuel utilization of 62.5% and an average composition of 50% H_2, 42% H_2O at the anode and 18.4% O_2 at the cathode. The nominal, single cell voltage of 0.78 V is chosen so that the stack operates at a power density of about 0.5 W cm^{-2}, which is an achievable performance for a methane-fueled SOFC. This voltage and power density corresponds to a current density of about 0.6 A cm^{-2}. The SOFC stack is sized and designed to operate at this nominal, single cell voltage while generating 1 MWe AC net power. Large-scale planar SOFC stacks are expected to employ cell areas as high as 625 cm^2 [15]. Based on the design voltage and the nominal power output, the size and number of stacks can be calculated:

$$P_{DC} = jA_{tot}V \tag{11}$$

where P_{DC} is near 1200 kWe DC to generate 1 MWe AC net power, j is determined from the modeled polarization curve and operating voltage, and A_{tot} is the total active area of the cells. Single cell performance is extrapolated to represent the SOFC stack. The number of cells and stacks can be determined as follows:

$$N_{cells} = \frac{A_{tot}}{A_{cell}} \tag{12}$$

$$N_{stacks} = \frac{N_{cells}}{cells\,per\,stack} \tag{13}$$

The purpose of the SOFC model is to generate the expected stack performance characteristics and its associated sensitivity to temperature, pressure, and compositional variations in the reactant feed gases. The actual size of the stack can be calculated from the model based on physical dimensions of the stack components. Table 2 shows the SOFC operating parameters of this model and a possible stack sizing calculation.

The power density of each cell is 0.48 W cm^{-2} based on the polarization curve and design voltage. The stack sizing scenario results in a gross dc power per stack of 60 kW, which requires 20 stacks to produce the 1200 kWe of dc power demanded by the plant.

2.5. Water–gas shift reactor

The anode effluent which is not recycled is cooled down to around 300 °C which is favorable for the WGS reaction. The anode tail-gas stream in the presence of a WGS catalyst is assumed to be in shift equilibrium in the model.

Table 2
SOFC operating conditions and stack sizing scenario.

T (°C)	727
U_f	0.62
V (V)	0.78
j (A cm^{-2})	0.62
P'' (W cm^{-2})	0.48
A_{cell} (cm^2)	625
Cells per stack	200
N_{cells}	3991
N_{stacks}	20

2.6. Hydrogen separation

The shifted gas stream is then fed into a hydrogen separation unit for which two separation methods are considered: EHS and PSA.

2.6.1. EHS (Concept 1)

The exact hydrogen separation amount and performance are unknown for large, commercial EHS modules, but performance can be estimated from previous sub-scale EHS stack tests. Mitlitsky [7] explored the performance of a prototype 15-cell EHS unit integrated with a 25 kW SOFC stack at two different SOFC fuel utilizations to determine the effect of hydrogen concentration on EHS operating voltage. The test results are shown in Fig. 5. The governing equations of the EHS unit which determine the power required for the specified hydrogen separation are shown in Eqs. (14) and (15).

$$i_{tot} = 2F\dot{n}_{H_2,tot} \tag{14}$$

$$P_{tot} = i_{tot}V_{cell} \tag{15}$$

This model conservatively estimates a 0.1 V cell voltage to separate 85% of the hydrogen from the shifted anode effluent based on the experimental findings of Mitlitsky [7] as shown in Fig. 5. The 0.1 V cell voltage estimation represents a 0.03 V increase in overpotential from the 0.07 V experimental cell voltage operation in which an SOFC fuel utilization of 70% was used; the overall SOFC fuel utilization in this model is 82.5%. It should also be noted that the estimated operating EHS stack voltage given in Fig. 5 is for comparative purposes only. The EHS stack simulated for integration with the 1 MW SOFC CHHP system is larger and will likely operate at a different current, but the same voltage.

2.6.2. PSA (Concept 2)

The shifted anode effluent is cooled down to 40 °C and the water content is purged prior to the PSA compressor inlet. The composition requirement for hydrogen at the inlet of the PSA unit is 70% or higher for the process to be economical and achieve 85% hydrogen separation with adequate purity (99.99+%) [5,6]. In order to achieve the 70% hydrogen content in the feed gas, a recycle of the separated hydrogen is employed, effectively lowering the overall hydrogen separation from 85% to 47% (84% of the separated hydrogen is recycled to the inlet to achieve 70%); this modeling approach is consistent with other work in the literature [5,6], and it is adequate for a high-level performance estimation of the PSA unit. Cost estimation for the PSA unit using this modeling approach requires the flow of separated hydrogen or tail gas [5,6]. The optimum feed pressure to the PSA ranges from 15 to 29 bar [5]; the inlet pressure for this model is chosen to be 18 bar.

It is noted that there are many PSA designs which are customized for certain separation processes, and detailed modeling of a PSA unit is complex and beyond the scope of the present work. This analysis uses a heuristic assessment with the goal of estimating the performance of low concentration hydrogen (40% dry) separation. Since the most common application of using a PSA unit for hydrogen

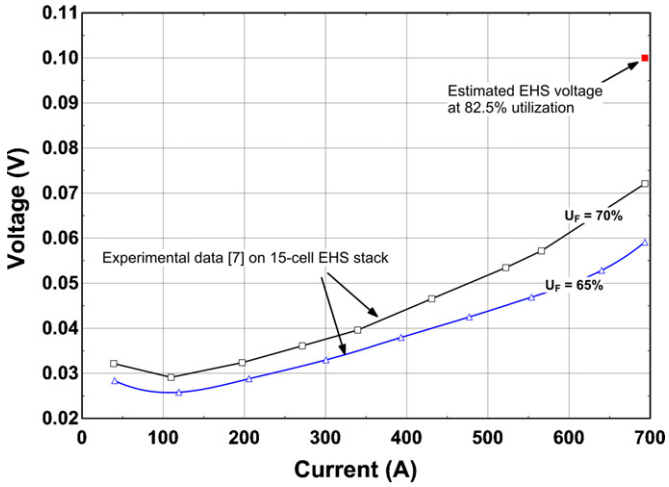

Fig. 5. EHS performance curve for U_f = 65% and U_f = 70%; data from Mitlitsky [7]. EHS performance point for this study with U_f = 85% is shown.

separation employs steam methane reformate streams having high (~75%) hydrogen compositions, the performance estimation of the PSA process in this study is extrapolated from a similar performance baseline: 85% separation for 70% hydrogen at the inlet. To operate continuously and achieve this degree of separation and product purity, multiple beds are required. It is estimated, following the methods given in a previous modeling study [16] with similar inlet gas conditions (mainly H_2 and CO_2), that four PSA beds are required for continuous operation while achieving 85% separation per pass.

2.7. Heat recovery

The hydrogen depleted tail gas is then fed into the combustor for heat recovery. If the energy in the depleted gas is not sufficient to raise the combustor effluent to 750 °C, excess methane is fed into the combustor. This is necessary to accomplish the preheat for fuel reforming. For this model, the higher overall hydrogen separation rate for the EHS required excess methane to be fed into the combustor. The PSA did not require excess methane because of increased hydrogen flow into the combustor (lower hydrogen recovery). As shown in Figs. 2 and 3, the design of the heat recovery loop is slightly different for the two separation methods. The water loop for Concept 1 flows through combustor effluent heat exchanger (HX-06) first, and then it recovers heat from the WGS effluent heat exchanger (HX-05) to cool the gas down to 190 °C for EHS operation. The water loop for Concept 2 flows through HX-05 first to maximize heat recovery, since the PSA inlet has to be cooled down much further (to 40 °C). A portion of the condensing process can be accomplished in the HX-05 by this design. The remaining heat rejection for condensing the PSA inlet stream is assumed to be accomplished with cooling water from a cooling tower (not shown in the concept figures and its presence is neglected in the current analysis).

2.8. Compressors

The efficiency of the compressors varies because of the different operating temperatures and compositions. Table 3 indicates the isentropic efficiency of the compressors which all have a mechanical efficiency of 95%. The water pump has a 99% mechanical efficiency. The anode recycle compressor operates at a low efficiency of 50% because of the high temperatures of the incoming gases (530 °C). Both the PSA compressor and the hydrogen product compressor require multiple stages because of an imposed pressure ratio limit of 2:1 with intercooling. The model assumes intercooling can be accomplished with negligible energy requirements (i.e., electric power for pumping cooling water to a heat exchanger). While this removes thermal energy from the gas streams, it makes the compression more efficient. By the same reasoning, the power required to cool and condense the gas stream for the PSA was also neglected, but this cooling results in a more significant heat recovery loss.

Table 3
Isentropic efficiencies of compressors and pump.

CH_4 compressor	75%
Air compressor	65%
Recycle compressor	50%
PSA recycle compressor	82%
H_2 compressor	82%
PSA compressor	75%
Water pump	85%

3. Model results

The model was simulated in Aspen Plus™ for the generation of thermodynamic performance characteristics. Two baseline operation cases were simulated which differed only in the method for hydrogen separation. The plant was designed to output a net power of 1 MWe AC, and the required fuel was calculated from the simulation. The hydrogen and heat generated downstream of the SOFC are byproducts, so the potential for recovery is dependent on the fuel utilization and efficiency of the SOFC. The feed rate of methane is the only energy input into the system, since the SOFC supplies the electrical needs of compression and EHS power. Some excess methane is fed into the burner to supply fuel preheating which cannot be accomplished by anode effluent recuperation. The outputs of the system are the net 1 MWe AC power, compressed hydrogen to 30 bar, and heat in the form of hot water (80 °C).

For Concept 1, the overall fuel efficiency is 85.2% based on the lower heating value (LHV) of hydrogen:

$$\eta_{\mathrm{CHHP}} = \frac{P_{net} + \mathrm{Heat} + \mathrm{LHV}_{\mathrm{H_2}}}{\mathrm{LHV}_{\mathrm{CH_4}}} \tag{16}$$

The electrical efficiency (LHV) is defined as:

$$\eta_{elec} = \frac{P_{net}}{\mathrm{LHV}_{\mathrm{CH_4}}} \tag{17}$$

The heat production efficiency (LHV) is defined as:

$$\eta_{heat} = \frac{\mathrm{Heat}}{\mathrm{LHV}_{\mathrm{CH_4}}} \tag{18}$$

The hydrogen production efficiency (LHV) is defined as:

$$\eta_{\mathrm{H_2}} = \frac{\mathrm{LHV}_{\mathrm{H_2}}}{\mathrm{LHV}_{\mathrm{CH_4}}} \tag{19}$$

The efficiencies defined in Eqs. (16)–(19) are shown in Table 4 for the two different plant concepts. The main differences between the two concepts are the hydrogen production and the electrical efficiency. The hydrogen production for Concept 1 is much higher due to the increased separation fraction of hydrogen for EHS compared to PSA; this is discussed in more detail below. The electrical efficiency for Concept 2 is higher than Concept 1 for two reasons: (1) Concept 2 does not require the combustion of excess methane for pre-heating the SOFC fuel and (2) the EHS compression energy for storing more hydrogen is higher. While the PSA unit separates less hydrogen, the combustible tail gas energy is sufficiently high to provide adequate fuel preheat.

The gross AC power of 1145 kW is required to provide a net output of 1026 kW, while supplying the internal electricity needs

Table 4
Baseline operating mode model results.

	Concept 1: EHS	Concept 2: PSA
Inputs		
Methane feed (kg s^{-1})	0.0420	0.0388
Methane LHV (MJ kg^{-1})	50	50
Methane HHV (MJ kg^{-1})	55.5	55.5
Fuel energy input LHV (kW)	2102	1941
Fuel energy input HHV (kW)	2333	2155
Internal power use (kW)		
CH_4 compressor	2	2
Air compressor	48	48
Recycle compressor	26	26
Heating water pump	0.5	0.5
H_2 compressor	17	2
EHS unit	27	
PSA compressor		48
PSA recycle compressor		0.4
Total internal power use (kW)	119	126
Losses		
Heat loss	52	48
DC/AC inversion loss	60	60
Energy outputs (kW)		
SOFC gross power kWe AC	1145	1145
Heat kWt	427	417
Hydrogen (kg day^{-1})	242	132
H_2 power LHV	338	185
H_2 power HHV	397	217
Gross output (Power, Heat, H_2) LHV	1911	1747
Gross output (Power, Heat, H_2) HHV	1969	1779
Net electric power output	1026	1019
Net energy output LHV	1791	1621
Net energy output HHV	1849	1653
Efficiency		
Electrical efficiency LHV	48.8%	52.5%
Electrical efficiency HHV	44.0%	47.3%
Heat production LHV	20.3%	21.5%
H_2 production LHV	16.1%	9.5%
Net total system efficiency LHV	85.2%	83.5%
Net total system efficiency HHV	79.3%	76.7%

for compression and EHS of 119 kW. The compression energy for the hydrogen product is subtracted from the net SOFC AC power production; considering this compression energy to be external to the system would increase the efficiency, especially in Concept 1 because more hydrogen is separated than in Concept 2.

In Concept 1, the EHS separates 85% of the hydrogen from its feed gas with the assumption of faradaic flows (i.e., 100% current efficiency) and an overpotential of 0.1 V. The total power required for hydrogen separation is about 27 kW which includes an internal compression of the hydrogen gas up to 33 kPa [1]; in essence this is a "free" compression because the voltage required for separation is also compressing the gas for no additional power input. The separated stream is purified to 1–2 ppm of CO based on the cathode reduction of CO stated in [5]: a high enough quality for PEM transportation fuel cells which are the likely recipient of the product hydrogen.

Concept 2 exhibits an 83.5% overall efficiency based on the LHV of hydrogen. The PSA unit can only recover about 47% of the hydrogen in the anode effluent. The PSA can only economically separate hydrogen if three criterion are met: the gas is at low temperatures (40–50 °C), the gas is dry, and the gas composition is above 70% [6]. The anode effluent must be cooled and drained of water before entering the PSA subsystem. About half of the heat loss due to PSA inlet gas cooling is recovered in the heating water loop, but the other half is lost to the environment; this loss partially offsets the additional heat from the excess hydrogen going into the combustor. For the composition requirement, a hydrogen recycle of the separated hydrogen coming out of the PSA is needed to bring the 40% hydrogen content in the water–gas shifted anode effluent up to 70% by volume. While each pass of the PSA separates 85% of the hydrogen, the required recycle of 84% brings the net hydrogen recovery down to about 47%.

The electric power required for hydrogen separation and storage compression are nearly equal for both concepts, but that is mainly because the PSA requires less power to store less hydrogen. In terms of energy per kg of hydrogen separated (storage compression energy not included), the EHS unit requires 2.7 kWh kg^{-1} H_2 while the PSA unit requires about three times more energy (8.2 kWh kg^{-1} H_2) to separate hydrogen from the shifted SOFC tail-gas.

Concept 1 requires an additional 160 kW of fuel to the combustor for SMR preheat which also increases the heat recovery. Both concepts generate in the neighborhood of 400 kW of thermal energy in the form of hot water which translates into a plant thermal-to-electric ratio of about 0.4. The chemical (hydrogen fuel)-to-electric ratio differs more substantially between concepts, with Concept 1 at 0.33 and Concept 2 at 0.18 on an LHV basis. As will be discussed, the amount of hydrogen production can be increased by increasing the fuel input to the plant without substantially increasing the electric power production via electrochemical fuel conversion.

3.1. Hydrogen over-production

An operational case study for this system was carried out to explore the effect of producing excess hydrogen. The requirement for each concept is to produce an extra 100 kg H_2 day^{-1} from the baseline case (Table 4). This requirement is met by feeding excess methane into the system, while the electric power requirement is still 1 MWe AC. All the component sizes, including the SOFC, remain the same. The excess methane fed into the system gets reformed in the SOFC subsystem, and the SOFC operating voltage increases slightly (10 mV) due to a higher content of reactant hydrogen (increases the Nernst potential) from a reduction in fuel utilization (from 63% to 54% per pass). Results from this scenario are given in Table 5.

The results from this case study show an increase in overall system efficiency for several reasons. Both scenarios increased operating voltage by about 10 mV, which slightly increased the SOFC efficiency. Despite this increase in operating voltage, both electrical efficiencies went down because of decreased fuel utilization. Slightly less compression power is required for the air blower (excess air is used for cooling the SOFC stack) in both concepts because the heat capacity of the anode gas increased. Concept 1 (EHS) required less additional methane for fuel preheat than the baseline case, even with the high amount of hydrogen recovery. Overall efficiency for Concept 2 (PSA) shows a greater increase than Concept 1 due to an increase in hydrogen separation efficiency; PSA recovery amount increased from 46.9% to 60.4% because of a higher hydrogen content in the feed gas of the PSA. The energy required for PSA hydrogen separation in Concept 2 was lowered to 5.8 kWh kg^{-1} H_2 (from 8.7), while the EHS unit in Concept 1 remained the same at 2.7 kWh kg^{-1} H_2. This is an expected increase in separation efficiency for the PSA unit because the anode effluent approaches a gas composition of a shifted methane reformate, for which PSA is mainly used.

PSA units are generally used in large-scale applications, such as hydrogen production for oil refineries, and the costs of PSA systems are not overly sensitive to capacity. Because of the increased performance for separation with low concentrations of hydrogen and the predicted cost advantage of EHS units based on the small-scale application, the EHS concept is chosen for the economic analysis.

Table 5
Hydrogen over-production case study model results.

	Concept 1: EHS	Concept 2: PSA
Inputs		
Feed rate (kg s^{-1})	0.0441	0.0417
Methane LHV (MJ kg^{-1})	50	50
Methane HHV (MJ kg^{-1})	55.5	55.5
Fuel energy input LHV (kW)	2206	2084
Fuel energy input HHV (kW)	2449	2313
Internal power use (kW)		
CH_4 compressor	2	2
Air compressor	42	43
Recycle compressor	28	28
Heating water pump	0.4	0.4
H_2 compressor	24	3
EHS unit	39	
PSA compressor		57
PSA recycle compressor		0.4
Total internal power use (kW)	135	133
Losses		
Heat loss	62	60
DC/AC inversion loss	61	61
Energy outputs (kW)		
SOFC gross power (kWe AC)	1160	1159
Heat (kWt)	392	417
Hydrogen (kg day^{-1})	345	238
H_2 power LHV	483	333
H_2 power HHV	566	390
Gross output (Power, Heat, H_2) LHV	2034	1908
Gross output (Power, Heat, H_2) HHV	2117	1965
Net electric power output	1025	1026
Net energy output LHV	1900	1775
Net energy output HHV	1983	1832
Efficiency		
Electrical efficiency LHV	46.5%	49.2%
Electrical efficiency HHV	41.9%	44.3%
Heat production LHV	17.7%	20.0%
H_2 production LHV	21.9%	16.0%
Net total system efficiency LHV	86.1%	85.2%
Net total system efficiency HHV	81.0%	79.2%

4. Economics

The economics of the Case 1 SOFC polygeneration plant (no H_2 over-production) are evaluated to determine the value of the hydrogen produced in a distributed generation scenario. In this section, capital, indirect, and operating and maintenance costs are formulated for the CHHP plant. Detailed cost estimation methods are given and the resulting economics are inputted into the H2A Tool developed by the National Renewable Energy Laboratory to estimate the cost of hydrogen and its sensitivity to prices in natural gas and electricity.

4.1. Capital investment

The capital investment requirement is first determined for the main subsystems of the plant, which include methane fuel and air preheat, 1.16 MW of SOFC gross ac electricity generation, 234 kg day^{-1} hydrogen production, and 427 kW of heat recovery. Multiple sources are used to determine the capital cost of the plant.

The capital costs of several of the system components are estimated using the cost scaling equation given in Eq. (20). The cost of each scaling unit (S) is based on the reference scaling unit (S_0) and base cost (C_0). The superscript n is the scaling factor which accounts for the economy of scale of a particular component. The cost is then adjusted for the time-dependent equipment cost changes using the Chemical Engineering Plant Cost Index (CEPCI). The installed cost (IC) is then calculated by using an installation factor (IF), which accounts for various costs associated with installing the component. Eq. (20) is used to calculate the installed cost based on the given parameters.

$$\mathrm{IC} = C_0 \left(\frac{S}{S_0}\right)^n \left(\frac{\mathrm{CEPCI}}{\mathrm{CEPCI}_0}\right) \mathrm{IF} \tag{20}$$

Table 6 gives the component cost breakdown of the plant. Reference costs are estimated from either scaling of literature data or via the economic analyzer within ASPEN Plus as given in the table footnotes. For example, the SOFC costs are estimated from recent DOE techno-economic studies [17] and scaled accordingly; whereas heat exchanger and blower costs are estimated directly from ASPEN Plus. In addition to direct costs, the indirect costs shown in Table 7 include engineering and design, plant construction, legal and contractors fees, and project contingencies; these costs were allocated based on Spath et al. [6]. The total capital investment (direct plus indirect costs) amounts to 4042 k$$_{2009}$, where it should be noted that this costing methodology results in an estimated accuracy of ±30%. The installed unit cost of the SOFC CHHP plant is then estimated to be about 3950 $ kWe^{-1} of net electric power generated.

4.2. Operating and maintenance costs

The operating costs for the plant were estimated using multiple sources and assumptions. The SOFC operating, maintenance, and replacement costs were estimated based on Gerdes et al. [17] to be 0.22 ¢ kWh^{-1}; the same assumption for operating the EHS unit is made. Table 8 gives the annual O&M costs for the major components of the plant. In addition to the total O&M in Table 8, the annual labor and overhead, licensing and permitting, insurance and taxes, and rent payments amount to 89.1 k$. Thus, the total annual O&M amounts to 168.9 k$ which translates into about 1.85 ¢ kWh^{-1} for a 90% capacity factor.

4.3. Methane feedstock and electricity credit rates

Energy Information Agency data from 2010 gives insight into the range for both methane feedstock and electricity credit rates. The range of natural gas rates for commercial consumers is roughly 7–15 $ MMBtu^{-1} (0.024–0.051 $ kWh^{-1}) on an HHV basis for the continental United States (30 $ MMBtu^{-1} for Hawaii), with the average at 10 $ MMBtu^{-1} (0.034 $ kWh^{-1}). Electricity rates range from 0.07 $ kWh^{-1} to 0.16 $ kWh^{-1} for the continental United States (0.29 $ kWh^{-1} for Hawaii), with the average at 0.10 $ kWh^{-1}.

The 400+ kW of thermal energy production is accounted for by assuming it is displacing hot water produced from a natural gas fired boiler which operates with 80% efficiency; this reduces the net cost of natural gas feedstock by an amount that is proportional to the heat production.

4.4. H2A life cycle analysis

The total capital investment (direct and indirect) for the plant is an input for the H2A life cycle analysis tool [21], which is used to generate a levelized cost for hydrogen production. The various economic parameters specified for the H2A program are given in Table 9. In particular, an internal rate of return of 10% is specified which makes the hydrogen production 'cost' values reported in this study more representative of a 'minimum selling price' or a 'hydrogen profited (or levelized) cost' [22]. Also, the operating capacity is assumed to be 90%; this is relatively high compared to larger-scale dedicated fuel production plants for two reasons: the plant is much smaller in scale (about 600 times smaller, cf. [23,6]) and the feedstock CH_4 can be easily stored at its source to deliver a continuous supply.

Table 6
Cost of system components in k$$_{2009}$.

	C_0[a]	S_0	S	Units	n	IF[b]	IC
SOFC and inverter[c]	0.53	1	1145	k$ kW^{-1}	–	1.42	858
Reformer[d]	204	1125	334	kg H_2 day^{-1}	0.7	1.1	96
WGS reactor[d]	169	1500	282	kg H_2 day^{-1}	0.7	1.1	58
EHS unit[e]	2.23	1	27	k$ kW^{-1}	–	1.42	85
Heat exchangers[f]	–	–	–	–	–	–	675
Blowers and pumps[f]	–	–	–	–	–	–	215
Burner[f]	–	–	–	–	–	–	248
H_2 compressor[g]	23	1	10	kg H_2 h^{-1}	–	2.47	155
Total installed costs[h]							2390
Total direct costs[i]							2677

[a] These base costs have been scaled from the original cost index ($CEPCI_0$) to the 2009 CEPCI (521.9).
[b] The installed factor is only used if the base cost does not include installation (otherwise its value is 1).
[c] Gerdes et al. [17]: cost of SOEC module of 400 $$_{2002}$ kW^{-1} uninstalled based on DOE cost target for SOFC systems including inverter and controls. An installation factor of 1.42 is also referenced.
[d] James [18]: H2A forecourt SMR derived H_2 case study; scaled based on kg H_2 day^{-1} produced.
[e] Saur [19]: based on a PEM electrolyzer cost of 2000 $$_{2005}$ kW^{-1}.
[f] AspenTech Economic Analyzer™ software is used to calculate the installed cost of floating head shell and tube heat exchangers based on heat transfer area (heat transfer coefficients calculated from P&T and materials suitable for the operating temperature (inconel was used for high temperature (>700 °C) operation), blowers and pumps based on flow rates and design pressure, and a high temperature burner based on heating duty and flow rate.
[g] James [18]: H2A forecourt SMR derived H_2 case study.
[h] The total installed cost (TIC) of the components is not inclusive of buildings and service facilities for the plant.
[i] The buildings and services facilities are estimated to be 12% of the TIC, adding 287 k$ to the installed component costs for the total direct costs.

Table 7
Indirect costs allocated as a percentage of TDC from Spath et al. [6] and actual costs for this plant.

	% of TDC	k$
Engineering and design	13	348
Site prep and construction	14	375
Legal and contractors fees	9	241
Project contingency	15	402
Total indirect costs	51	1365

It should also be noted that the cost estimated with the H2A tool does not include compression, storage, and dispensing of hydrogen. In this study, the CH_4 feedstock is converted to an equivalent natural gas cost on an LHV basis for use in the H2A tool. A range of methane feedstock cost is explored to account for both the dynamic nature of and the geographic variation in natural gas prices throughout the United States. The value of electricity co-product is also varied for the same reason and to gain an understanding of its influence on hydrogen production cost.

Table 8
Operating costs for various components.

	Annual k$
SOFC[a]	20.9
Reformer catalyst[b]	13.3
WGS reactor catalyst[c]	4.7
EHS unit[d]	0.5
Unplanned[e]	40.4
Total[f]	79.9

[a] Gerdes et al. [17]: 0.0022 $ kWh^{-1} of SOFC AC_e production.
[b] James [18]: reactor sizing from 20,000 GHSV with 7 $$_{2005}$ lb-cat^{-1}. Assumed catalyst density of 1200 kg m^{-3}. Catalyst replaced every year.
[c] James [18]: reactor sizing from 10,000 GHSV with 7 $$_{2005}$ lb-cat^{-1}. Assumed catalyst density of 1200 kg m^{-3}. Catalyst replaced every year.
[d] Assumed same operating costs as SOFC (0.0022 $ kWh^{-1} for DC power input to EHS).
[e] Unplanned O&M assumed to be 1% of the production TDC based on Steward and Penev [20].
[f] This total is not inclusive of labor and overhead, insurance and taxes, licensing and permitting, and property rental.

4.5. Hydrogen production cost sensitivity analysis

The estimated cost of hydrogen using the H2A tool ranges from 1.8 $ kg^{-1} to 7.2 $ kg^{-1} depending on the cost of the natural gas feedstock as shown in Fig. 6. Recall that 1.03 MW of ac electricity and 427 kW of thermal energy co-products are exported from the system to generate such hydrogen cost estimates. A breakdown of cost contributions to the total cost of hydrogen produced from this system in $ kg^{-1} is also shown for a constant electricity credit of 0.10 $ kWh^{-1}. The capital costs are the most significant contributor when the methane feedstock costs are low (below 8 $ MMBtu^{-1}). The methane feedstock cost contribution dominates when the costs are high, and the hydrogen production costs rise quickly for a constant electricity credit price of 0.10 $ kWh^{-1}. As the methane feedstock costs increases, the heat production credit also increases which decreases the rate at which hydrogen production costs go up. The O&M costs add about 2 $ kg^{-1} to the hydrogen production costs.

Table 9
Economic inputs to the H2A tool.

	Value
Constant dollar value	2005
Internal rate of return (after-tax)	10%
Debt/equity	0%/100%
Plant life	20 years
Depreciation	MACRS
Depreciation recovery period	7 years
Construction period	1 year
1st year	100%
2nd year	0%
Start-up time	6 months
Revenues	50%
Variable costs	75%
Fixed costs	100%
Working capital	15% of total capital investment
Inflation rate	1.90%
Total taxes	38.90%
Decommissioning costs	10% of depreciable capital
Salvage value	10% of total capital investment
Operating capacity	90%
CH_4 feedstock cost	Varied
Electricity product price	Varied
Heat product cost	Equivalent to CH_4 feedstock
Hydrogen product cost	Output

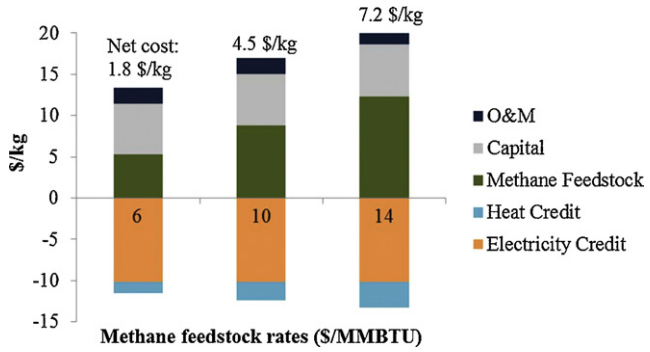

Fig. 6. Hydrogen production costs and contributions for an electricity credit price of 0.10 $ kWh^{-1} at various methane feedstock costs.

Fig. 7 further explores the dependence of hydrogen production cost on the methane feedstock costs at various electricity credit prices. The cost of hydrogen has an increasing linear dependence on the methane feedstock cost, as shown in the figure. For the electricity credit of 0.12 $ kWh^{-1}, the hydrogen production cost ranges from 0 to 6.5 $ kg^{-1} for the methane feedstock cost of 6–16 $ MMBtu^{-1}. Interestingly, the figure shows that for each 1 $ MMBtu^{-1} (0.0034 $ kWh^{-1}) of methane feedstock cost, the hydrogen production cost increases by about 0.67 $ kg^{-1}. For an electricity credit of 0.08 $ kWh^{-1} and a methane feedstock cost of 6 $ MMBtu^{-1} (0.021 $ kWh^{-1}), the cost of hydrogen production is about 4 $ kg^{-1}, and it rises to about 11 $ kg^{-1} for a high methane feedstock cost of 16 $ MMBtu^{-1} (0.055 $ kWh^{-1}).

Fig. 8 illustrates the dependence of hydrogen production cost on the electricity credit prices at various methane feedstock costs. The cost of hydrogen production has a decreasing linear dependence on the electricity rate. The hydrogen production cost ranges from 12 $ kg^{-1} to essentially free for an electricity credit price range of 0.04–0.16 $ kWh^{-1}. Thus, for each 0.01 $ kWh^{-1} of electricity credit, the hydrogen production cost decreases by about 1 $ kg^{-1}. For a methane feedstock cost of 12 $ MMBtu^{-1} (0.041 $ kWh^{-1}) and an electricity credit price of 0.10 $ kWh^{-1}, the cost hydrogen is 5.9 $ kg^{-1}. For a methane feedstock cost of 16 $ MMBtu^{-1} (0.055 $ kWh^{-1}), the hydrogen cost ranges from 10.7 $ kg^{-1} to 2.3 $ kg^{-1} for the range of electricity credit prices shown.

The cost of producing hydrogen from the SOFC CHHP system is highly dependent on both the methane feedstock cost rate and the electricity product value. This is consistent with the economic trade-offs of fuel and power producing systems: higher value products and lower value feedstock will result in favorable economics.

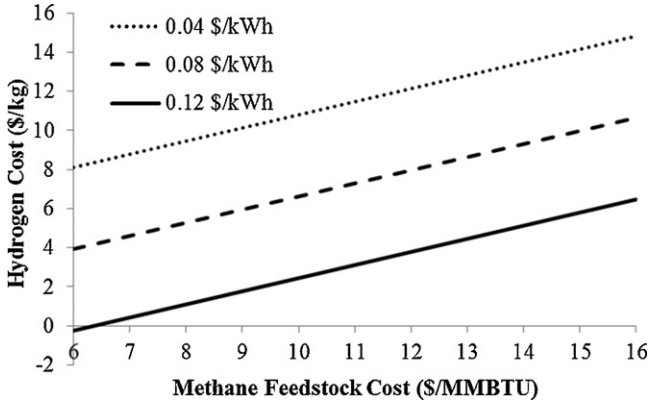

Fig. 7. Cost of hydrogen production dependency on methane feedstock costs for various electricity credit prices.

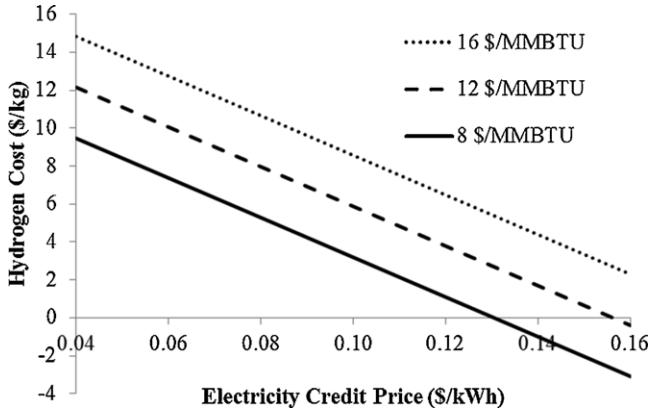

Fig. 8. Cost of hydrogen production dependency on electricity credit prices for various methane feedstock costs.

The so-called 'spark spread[1]' is the difference between the cost of electricity (in ¢ kWh^{-1}) and natural gas (in $ MMBtu^{-1}), and it is indicative of the economic viability of using fuel cell systems in distributed generation applications. As a rule of thumb, the spark spread should be greater than two for fuel cell systems to be cost effective; this is also necessary for the hydrogen production cost to be low. The cost of hydrogen is as low as 2.4 $ kg^{-1} when the electricity price is 12 ¢ kWh^{-1} and the methane feedstock cost is 10 $ MMBtu^{-1} (0.034 $ kWh^{-1}); dropping the cost of the methane feedstock down to 9 $ MMBtu^{-1} (spark spread of three) brings the hydrogen production cost down to 1.77 $ kg^{-1}.

There are several important conclusions to draw from these results. First, it is apparent from Fig. 8 that at electricity prices of 13 ¢ kWh^{-1} and gas prices of 8 $ MMBtu^{-1} (0.027 $ kWh^{-1}) or less, the hydrogen cost approaches a value of 0 $ kg^{-1} to achieve a 10% rate of return. Thus, 'spark spreads' of five or more offer near-zero or negative hydrogen production costs for CHHP plant costs assumed in this study. Second, it has been noted that the unit cost of hydrogen should be lower for fuel cell-based distributed polygeneration systems, due to the allocation of capital among all of the co-products. This claim is examined more closely by comparing hydrogen production costs at multiple scales via other pathways as shown in Table 10. Large-scale production costs via steam methane reforming (SMR) of natural gas have been estimated at about 1.40 $ kg^{-1} (in 2005 US$) and typically serve as a baseline for alternative pathway cost comparisons. At distributed-scales (~250 kg day^{-1}), SMR-based hydrogen production cost has been estimated at 3.5 $ kg^{-1} and around 4.17 $ kg^{-1} for distributed electrolysis plants (~1050 kg day^{-1} scale). Interestingly, molten carbonate fuel cells (MCFCs) co-producing heat, hydrogen, and power without any government incentives is estimated to generate hydrogen at about 4.6 $ kg^{-1}. In the present study, the SOFC CHHP plant generates hydrogen at a comparable cost of 4.4 $ kg^{-1}, which is about 5% lower than an MCFC CHHP plant and 25% higher than SMR-based hydrogen production. As with distributed electrolysis systems, hydrogen production from fuel cell-based CHHP plants is sensitive to grid electricity prices (sell-back). Thus, fuel cell-based polygeneration plants are shown to have hydrogen production costs that are on par with conventional and alternative pathways (although not necessarily cheaper) while providing power and thermal energy services.

[1] Spark spread is often represented with electricity and gas prices sharing the same units of $/MWh. For sake of convenience, the spread is represented here with differing units to allow for small round numbers. Note that a spread of '2' used herein equals a value of 86 $/MWh when using the same units for electricity and fuel.

Table 10
Comparison of hydrogen production costs.

Hydrogen production pathway	$ kg^{-1}
SMR of natural gas (large-scale[a])	1.4 [6]
Biomass to H_2 (large-scale[a,c])	1.6 [6]
SMR of natural gas (distributed-scale[b,f])	3.5 [24]
Electrolysis (distributed-scale[b,f])	4.17 [26]
MCFC CHHP system (distributed-scale[b,d,e,f])	4.6 [24]
SOFC CHHP system (distributed-scale[b,d])	4.4

[a] Large-scale hydrogen production is on the order of ~150,000 kg day^{-1}.
[b] Distributed-scale hydrogen cost is estimated from ~250 kg day^{-1} production values (1050 kg day^{-1} for electrolysis).
[c] Biomass feedstock cost is $50 per dry metric ton.
[d] Price of natural gas feedstock is $7 MMBtu^{-1} (0.024 $ kWh^{-1}) and electricity sell-back of 8.2 ¢ kWh^{-1}.
[e] MCFC capital cost = $2500 kW^{-1} (uninstalled) and without incentives [22].
[f] Distributed scale hydrogen cost subtracts out an estimated 4.03 $ kg^{-1} for compression, storage, and dispensing [25] for SMR, MCFC CHHP, and 1.88 $ kg^{-1} for electrolysis [26].

Hydrogen fuel cell vehicles can achieve between 50 and 70 miles kg^{-1} of hydrogen; this is almost double the fuel economy, in miles per gallon of gasoline, compared to a gasoline powered car. The value of hydrogen in $ kg^{-1} can be competitive with gasoline at prices slightly above the selling price of gasoline (3–4 $ gal^{-1}) for this reason. Setting up a fueling station for fuel cell vehicles near the SOFC CHHP system would add costs to the production of hydrogen.

5. Conclusions

This study aimed to demonstrate the potential benefits of an SOFC system for energy co-generation. The unique aspect of this plant, compared to other co-generating fuel cell systems, is the separation of hydrogen which could be used for end uses such as PEM fuel cell-powered vehicles. SOFC systems with co-generation are known to exhibit high overall efficiency, and this study characterized the potential for a relatively new technology (EHS) to separate hydrogen from SOFC effluent gas streams. The overall fuel efficiency of 85.2% LHV is relatively high, and the value of PEM fuel cell grade hydrogen could make this type of a system even more desirable.

There are several trade-offs between the two methods for hydrogen separation. The PSA system is a commercially developed separation method, but the performance suffers from a low concentration of H_2 in the anode effluent stream. This results in a low overall hydrogen separation rate of less than 50% for the baseline case. While ESA units are less commercially available, they use less electricity based on the assumed overpotential of 0.1 V, and the separation rate of 85% is much higher.

The case study for hydrogen overproduction results in increased overall efficiency for both concepts. The PSA efficiency shows a greater increase due to the increase in hydrogen content for the PSA, but the EHS concept still has higher efficiency (both hydrogen and overall). The increase in hydrogen recovery and a higher overall efficiency makes the EHS unit a better option than PSA for SOFC effluent hydrogen separation.

The economics of this process were evaluated to determine the value of the hydrogen produced in a co-generation plant. For the electricity credit of 0.08 $ kWh^{-1} and a methane feedstock cost of 6 $ MMBtu^{-1}, the cost of hydrogen production is about 4 $ kg^{-1}, and it rises to about 11 $ kg^{-1} for a high methane feedstock cost of 16 $ MMBtu^{-1}. For each 1 $ MMBtu^{-1} of methane feedstock cost, the hydrogen production cost increases by about 0.67 $ kg^{-1}. For a methane feedstock cost of 10 $ MMBtu^{-1} and an electricity credit price of 0.12 $ kWh^{-1} (spark spread of 2), the cost of hydrogen is 2.4 $ kg^{-1}. For each 0.01 $ kWh^{-1} of electricity credit, the hydrogen production cost increases by about 1 $ kg^{-1}. The economic findings in this study show that hydrogen production costs are highly dependent on the spark spread of methane and electricity, but that CHHP plants are capable of producing hydrogen at production costs that are on par with other distributed production pathways, such as SMR of natural gas and electrolysis. Analyses for future work include the effects of system "turndown," for which less electric power and hydrogen are produced, and the associated economic implications of reduced plant capacity factor.

Acknowledgements

The authors would like to thank the National Renewable Energy Laboratory for financial support under Award#: KXEA-3-33607-54 and Darlene Steward for helpful information on the NREL Fuel Cell Power Tool runs related to molten carbonate fuel cell CHHP studies.

References

[1] M. Thomassen, E. Sheridan, J. Kvello, J. Nat. Gas Sci. Eng. 2 (5) (2010) 229–234.
[2] K.A. Perry, G.A. Eisman, B.C. Benicewicz, J. Power Sources 177 (2) (2008) 478–484.
[3] G. Eisman, D. Neumann, B.C. Benicewicz, A.M. Galeano, H_2 Pump, LLC, <http://www.h2pumpllc.com/5.html> (accessed 2011).
[4] M.K. Mann, Technical and Economic Assessment of Producing Hydrogen by Reforming Syngas from the Battelle Indirectly Heated Biomass Gasifier, TP-431-8143, National Renewable Energy Laboratory, Golden, CO, 1995.
[5] S.M. Leiby, Options for Refinery Hydrogen, SRI Report No. 212, Menlo Park, CA, 1994.
[6] P. Spath, A. Aden, T. Eggeman, M. Ringer, B. Wallace, J. Jechura, Biomass to Hydrogen Production Detailed Design and Economics Utilizing the Battelle Columbus Laboratory Indirectly-Heated Gasifier, TP-510-37408, National Renewable Energy Laboratory, Golden, CO, 2005.
[7] F. Mitlitsky, Low-cost Co-production of Hydrogen and Electricity, DOE Hydrogen Energy Program FY 2008 Annual Progress Report, Presented at the 2008 DOE Annual Merit and Peer Review, 2008. Available from: http://www.hydrogen.energy.gov/pdfs/progress08/v_d_6_mitlitsky.pdf.
[8] N. Perdikaris, K.D. Panopoulos, P. Hofmann, S. Spyrakis, E. Kakaras, Int. J. Hydrogen Energy 35 (6) (2010) 2446–2456.
[9] P. Lisbona, A. Corradetti, R. Bove, P. Lunghi, Electrochim. Acta 53 (4) (2006) 1920–1930.
[10] S. Campanari, P. Iora, J. Power Sources 132 (1–2) (2004).
[11] R. Bove, P. Lunghi, N.M. Sammes, Int. J. Hydrogen Energy 30 (2) (2005) 181.
[13] P. Costamagna, A. Selimovic, M.D. Borghi, G. Agnew, Chem. Eng. J. 102 (1) (2004) 61.
[14] R.P. O'Hayre, S.W. Cha, W. Colella, F.B. Prinz, Fuel Cell Fundamentals, John Wiley & Sons, Inc., New York, USA, 2009.
[15] K. Lai, B.J. Koeppel, K.S. Choi, K.P. Recknagle, X. Sun, L.A. Chick, V. Korolev, M. Khaleel, J. Power Sources 196 (6) (2011) 3204–3222.
[16] D. Nikolic, A. Giovanoglou, M.C. Georgiadis, E.S. Kikkinides, Hydrogen Purification by Pressure Swing Adsorption, PRISM EC Contract Number MRTC-CT-2004-512233, 2004.
[17] K. Gerdes, E. Grol, D. Keairns, R. Newby, Integrated Gasification Fuel Cell Performance and Cost Assessment, DOE/NETL-2009/1361, March, 2009.
[18] B.D. James, H2A Hydrogen Production Analysis Software Case Study: Current (2005) Steam Methane Reformer at Forecourt 1500 kg/day, National Renewable Energy Laboratory, 2009, Available from: http://www.hydrogen.energy.gov/h2a_production.html.
[19] G. Saur, Wind-To-Hydrogen Project: Electrolyzer Capital Cost Study, National Renewable Energy Laboratory, Technical Report, NREL/TP-550-44103, U.S. DOE, Golden, CO, 2009.
[20] D. Steward, M. Penev, FCPower CHP Production Analysis Software Case Study: Molten Carbonate Fuel Cell Case Study, National Renewable Energy Laboratory, Golden, CO, 2009, Available from: http://www.hydrogen.energy.gov/fc_power_analysis.html.
[21] D. Steward, T. Ramsden, J. Zuboy, H2A Production Model, Version 2 User Guide, National Renewable Energy Laboratory, Technical Report, NREL/TP-560-43983, 2008.
[22] D. Steward, M. Penev, Fuel Cell Power Model: Evaluation of CHP and CHHP Applications, 2010 Vehicle Technologies and Hydrogen Programs, Annual Merit Review and Peer Evaluation Meeting, U.S. Department of Energy, June 7–11, Washington, D.C., 2010. Available from: http://www.hydrogen.energy.gov/.
[23] R.J. Braun, L.G. Hanzon, J.H. Dean, ASME J. Energy Res. Technol. 133 (012601) (2011), doi:10.1115/1.4003541.
[24] F. Joseck, Systems Analysis, 2010 Vehicle Technologies and Hydrogen Programs, Annual Merit Review and Peer Evaluation Meeting, U.S. Department of Energy, June 7–11, Washington, D.C., 2010. Available from: http://www.hydrogen.energy.gov/.
[25] D. Steward, Comparison of Various Strategies for Small Scale Production of Hydrogen, Internal Report, National Renewable Energy Laboratory, Golden, CO, December 2009, personal communication, July 2011.
[26] M.F. Ruth, V. Diakov, M. Laffen, T.A. Timbario, FuelCell2010-33185, Proc. of ASME 8th International Fuel Cell Science, Engineering, and Technology Conference, June 14–16, Brooklyn, NY, 2010.